energies

Article

Optimum Design and Performance Analysis of Superconducting Cable with Different Conductor Layout

Sisi Peng [1,2], Chuanbing Cai [1,3,*], Jiaqi Cai [2], Jun Zheng [2] and Difan Zhou [1,3]

1 Department of Physics, Shanghai University, Shanghai 200444, China
2 Wuhan Institute of Marine Electric Propulsion, Wuhan 430064, China
3 Shanghai Key Laboratory of High Temperature Superconductors, Shanghai Frontiers Science Center of Quantum and Superconducting Matter States, Department of Physics, Shanghai University, Shanghai 200444, China
* Correspondence: cbcai@shu.edu.cn

Abstract: Compared with the traditional cable, the high-temperature superconducting (HTS) cable has the advantages of low loss and large capacity transmission. At present, the research on HTS cables mainly focuses on the calculation of AC loss, the performance under specific working conditions and cooling system design. Relatively little research has been carried out on the basic design and overall layout optimization of the cables. In this paper, an HTS cable with a rated current of 4 kA was designed. Firstly, according to the selected superconducting cable parameters, the body design of cables with different structures was carried out and the corresponding finite element models were built. Then, the performance analysis of HTS cables with different layouts was carried out based on the proposed cable performance evaluation indicators and the CORC double-layer structure was determined as the scheme of this cable. Finally, the AC loss of the cable with this topology was calculated to be 9.81 J/m under rated conditions. The cooling system can ensure the safe operation of the cable in the rated temperature range.

Keywords: HTS cable; topology; CORC; AC loss

check for updates

Citation: Peng, S.; Cai, C.; Cai, J.; Zheng, J.; Zhou, D. Optimum Design and Performance Analysis of Superconducting Cable with Different Conductor Layout. *Energies* **2022**, *15*, 8893. https://doi.org/10.3390/en15238893

Academic Editor: Pietro Romano

Received: 1 November 2022
Accepted: 22 November 2022
Published: 24 November 2022

1. Introduction

Since the discovery of high-temperature superconductors in 1986, many countries have invested a lot of money in research on high-temperature superconducting (HTS) cables [1–3]. Compared with the traditional copper cable, the HTS cable has the characteristic of zero resistance; its total loss during operation is only half of the conventional loss. The current transmission capacity of the HTS cable under the same cross-sectional area is 3–5 times that of the conventional cable, which can improve the transmission capacity of the cable. What is more, HTS cables are environmentally friendly and can withstand higher short-circuit currents, which is of great significance for improving the stability of power system operation.

At present, the research on HTS cables mainly focuses on the calculation of AC loss, the performance under specific working conditions and the cooling system design of superconducting cables. Lee [4] calculated the alternating current (AC) loss of the tri-axial HTS power cable by using an FEM program based on the Maxwell equation and the result was used to confirm the AC loss of the tri-axial HTS power cable prototype measured by the electrical measurement method. Nguyen [5,6] proposed a multilayer HTS power cable model that used a Cu-former layer in each phase for transient study and presented a fault analysis of the co-axial HTS cable in the mesh system. Lee [7] conducted a longitudinal temperature analysis according to the structure of the refrigerant circulation system of the cable and proposed a refrigerant circulation system. Choi [8] described the thermo-hydraulic analysis of the triaxial HTS power cable to determine the proper mass flow rates of subcooled liquid nitrogen that meet the operating temperature and pressure of the cable for four configurations of cooling systems. Huang [9] proposed a new structure of cable composed of many three-phase groups, which decomposes the superconducting layers into many magnetically independent three-phase groups. The new architecture greatly reduces the AC loss and the efficiency of reducing loss is enhanced with the increase of layers. Inoue [10] devised an HTS cable termination applying a wireless power transmission (WPT) system. The WPT system for the HTS cable termination can mechanically separate the HTS cable (low temperature part) from the copper cable (normal temperature part). Sadeghi [11] studied the electrothermal performance of a 22.9 kV HTS AC cable under transients such as short circuit faults and Islanding Operating Mode (IOM) of a wind farm. Keun Oh [12] introduced a new concept of H-formulation to reformulate the self-consistent static current model which has been devised to evaluate the critical current of high-temperature superconducting conductors. Jacob [13] conducted a comparative life cycle assessment of two different types of cooling systems for a 1 km long, 10 kV concentric three-phase high-temperature superconducting cable. Tang [14] developed a cryogenic refrigeration system combining open and closed refrigeration for 35 kV/2000 A HTS cables.

It can be seen that the current research involves less basic design and overall layout optimization for the cable. Therefore, it is necessary to compare the design schemes of different layout of HTS cables, select a better scheme for layout optimization and design a complete topology scheme of HTS cables. In this paper, an HTS cable with the rated current of 4 kA was designed. Firstly, the characteristics of superconducting tapes were summarized and on this basis, the basic parameters of HTS cables were determined. Then, the performance analysis of HTS cables with different conductor layouts was carried out and the CORC double-layer structure was determined as the scheme of this cable. Finally, the AC loss of the cable with this topology was calculated. While many studies have compared the characteristics of different cables on a macro scale, this paper focuses on a specific cable and compares the electromagnetic characteristics of cables with different topologies to provide guidance for design.

2. Properties of HTS Tapes

2.1. The Flow Capacity of HTS Tapes under Different Temperatures

Figure 1 shows the critical current and n of the second-generation HTS tape PA1212 produced by the Shanghai Superconducting Company at different temperatures [15]. n is also an important parameter for the current-carrying properties of superconductors, reflecting how quickly they change from the superconducting to the normal state, shown in Formula (1). It can be seen that as the ambient temperature decreases, the critical current of the superconducting tape in the same magnetic field environment gradually increases and the value of n increases firstly and then gradually decreases to 0.

$$E = E_c(I/I_c)^n \tag{1}$$

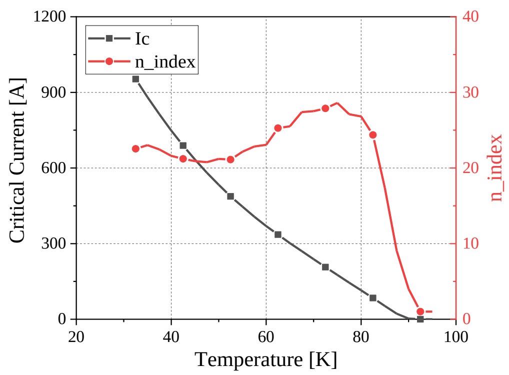

Figure 1. Critical current of PA1212 2G HTS tape at different temperatures.

2.2. Anisotropy of Superconducting Tapes

The flow capacity of HTS tapes is greatly affected by the magnetic field environment in which it is located and has strong anisotropy. In addition, when artificial pinning centers (APCs) are created, the critical current may not be consistent over the length of the tape [16,17]. Figure 2 shows the magnetic field distribution on the surface of the superconducting tape. For the same magnitude of the magnetic field, the degradation of critical current of the superconducting tape caused by the vertical magnetic field is significantly greater than that of the parallel magnetic field. In practical applications, the magnetic field environment in which the superconducting tape is located is very complex and the magnetic fields of different directions and strengths will have different effects on the flow capacity of the superconducting tape. Different from superconducting equipment with extremely high power density such as superconducting magnets, the highest magnetic field of superconducting cables under different operating conditions is only tens or hundreds of mT. Considering the most severe vertical field situation, in the cold helium and liquid nitrogen temperature range where the cable may operate, the critical current of PA 1212 2G HTS tape of the Shanghai Superconducting Company is shown in Figure 3.

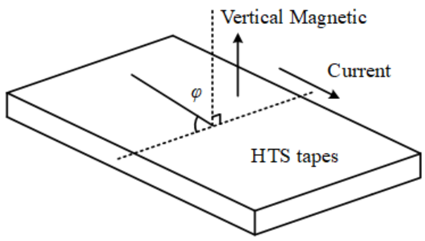

Figure 2. Magnetic field on the surface of superconducting tape.

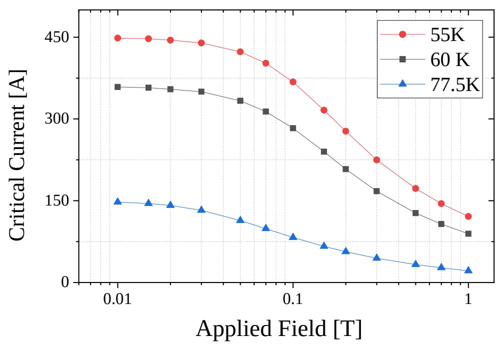

Figure 3. Critical current of PA1212 2G HTS tape under vertical fields.

3. Preliminary Design of HTS Cable

3.1. The Parameters of 4 kA HTS Cable

(1) Superconducting cable operating temperature range

The current-carrying capacity of superconducting cables mainly depends on the operating temperature range of the cable. The main refrigerant is liquid nitrogen, which is widely used in various HTS cable projects. A limiting factor for liquid nitrogen is its temperature, which can only reach 63 K before solidifying at ambient pressure. Liquid refrigerant travels through confined space; leakage of it may cause suffocation. Liquids have a much higher heat capacity than gases, so a rupture of a cryostat may also cause "cold burns" to nearby personnel and equipment. Considering safety, weight and the system operating temperature requirements, the selected refrigerant is gaseous helium, even though it is more expensive.

The optimum operating temperature of the cable is determined on the basis of comprehensive consideration of factors such as refrigeration requirements, current-carrying capacity and required cryostat size. As an obvious driver of all parameters, the ideal temperature for the cable is around 60 K.

(2) Number of tapes

The number of tapes required for the superconducting cable is mainly determined by the current-carrying capacity of the cable. The number N of superconducting tapes required for superconducting cables should satisfy Formula (2):

$$N \geq k_1(1 + k_2)I_R/k_3 I_c \tag{2}$$

where I_c is the critical current of the superconducting tape under the operating temperature and self-field of the cable; I_R is the rated line current of the cable; k_1 is the cable operation mode, 1 for the DC cable and 2 for the AC cable; k_2 is the design margin factor, including the critical current degradation caused by the winding process, the uneven current distribution of the tape and the safety margin; k_3 is the degradation coefficient of the critical current due to the magnetic field [18].

Under the current processing conditions, the degradation of the critical current of the superconducting tape after winding can be controlled within 5%; reasonable parameter design can realize the current equalization between layers; when the cable carries current, the tape is mainly affected by the magnetic field parallel to the surface of the tape, which has little effect on the critical current, so k_3 takes 1. Considering the above factors comprehensively and ensuring a certain safe operating margin, the margin coefficient k_2 of the superconducting cable operation is taken as 1. Therefore, the number of tapes required at different operating temperatures, calculated according to Formula (2), is shown in Figure 4.

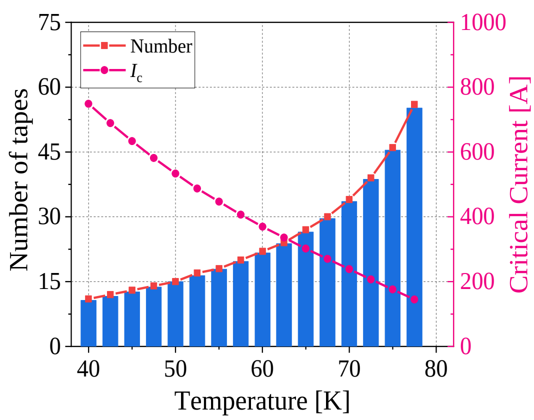

Figure 4. Quantity of PA1212 2G HTS tapes required in different temperature.

Combined with the selection of the cable operating temperature range, when using 60 K gaseous helium as the refrigerant, the required number of HTS tapes is at least 22.

(3) Number of conductor layers

The conductor layout and the number of conductor layers of the superconducting cable are important structural parameters of the cable. Since the cable mainly operates in DC mode, there is no current distribution problem between layers, so it is not necessary to design the current distribution of the conductors. However, if all superconducting tapes are arranged in parallel or on the same layer, the size of the cable will inevitably be too large. This will lead to an increase in the amount of wire used for the superconducting tape during the cable winding process and will also reduce the cooling efficiency of the cable body. In order to improve the current density of the superconducting cable, the conductor of the superconducting cable generally adopts a multi-layer layout.

(4) Electrical insulation design

The main insulation structure of conventional cables can be divided into winding type and extrusion type according to different molding methods. Compared with the extruded insulation cable, the winding insulation cable is more flexible and the internal stress is much smaller, especially in the low temperature environment of liquid nitrogen. Therefore, the superconducting cable with cold insulation structure is generally insulated with a winding structure.

Considering the wrapping process and economy of the insulating material, the cable uses polyimide as the insulating material and is wrapped in a single layer with a thickness of 0.1 mm.

(5) Cable cross-sectional area

Unlike normal cables, superconducting cables have minimal voltage drop and loss. So, the design of superconducting cables does not need to consider the influence of rated voltage and cable length on the energized cross-section.

3.2. 4 kA HTS Cable Design

The different stacking methods of superconducting tapes have a great influence on their electromagnetic and mechanical properties. A variety of superconducting conductor structure design methods based on second-generation high-temperature superconducting tapes have been proposed. Common conductors include CORC, Roebel, TSTC, CICC, HTS-CroCo and quasi-isotropic HTS strands. The diagram of different cables is shown in Figure 5. They all improve the electromagnetic and mechanical properties of conductors to a certain extent.

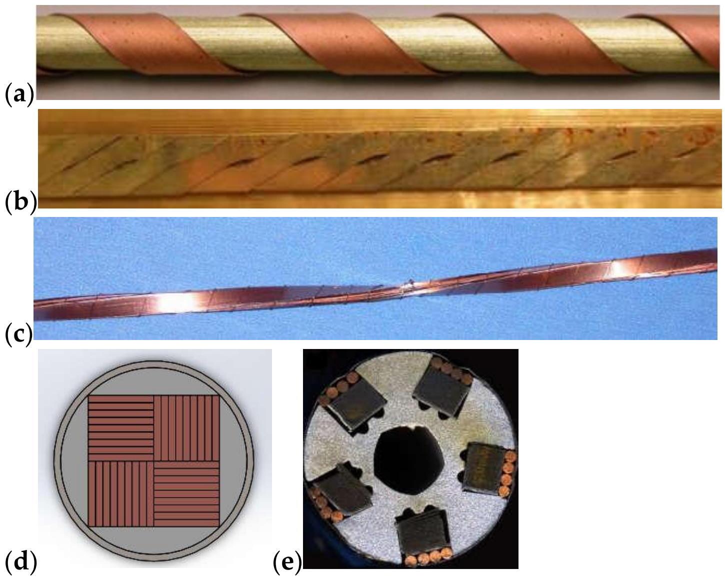

Figure 5. Diagram of the cables. (**a**) CORC; (**b**) Roebel; (**c**) TSTC; (**d**) Quasi-isotropic HTS strands; (**e**) CICC.

(1) CORC

CORC cables have the advantages of high current-carrying capacity, isotropic mechanical and electromagnetic properties and high mechanical flexibility. They are constructed by spirally winding superconducting tapes around the core and wrapping them with the insulating material on the outside [19]. The schematic diagram of the conductor layer is shown in Figure 6.

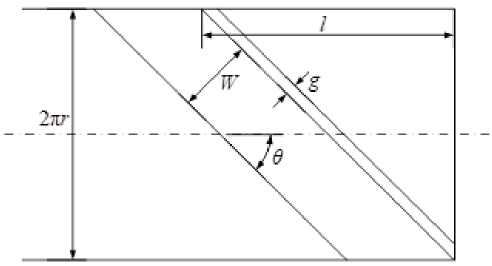

Figure 6. Schematic diagram of the conductor layer.

The winding radius of the conductor layer is related to the number of superconducting tapes contained in the conductor layer and the winding angle of the conductor layer. The width W of the superconducting tape, the width g of the gap between the tapes, the winding pitch l of the tape, the winding radius r, the winding angle θ and the number of superconducting tapes contained in the conductor layer N satisfy Formulas (3) and (4).

$$N \cdot \frac{W+g}{\cos\theta} = 2\pi r \tag{3}$$

$$l = \frac{2\pi r}{\tan\theta} \tag{4}$$

The outer conductor radius is the sum of the inner conductor radius r, the thickness of the superconducting tape h_{tape} and the insulation thickness t. The width W of the superconducting tapes is 4 mm; the average gap width g between the tapes is 0.5 mm. If the winding angle is too large, the amount of superconducting tapes will increase sharply; if the winding angle is too small, asymmetric stress concentration will easily occur at the bend of the cable. Therefore, the winding angle of the conductor layer is limited between 20° and 35°. For the degaussing cable, the external magnetic field of the cable must be large enough, which requires the axial current of the cable to be large enough and the winding angle of the conductor layer to be relatively small. Therefore, the winding angle θ is designed to be 20°. If the cable adopts a double-layer CORC structure, the number of tapes of both inner and outer layers is 11; the radii of the inner and outer conductors are 8.4 mm and 8.9 mm, respectively.

(2) Roebel

The Roebel cable is mainly used to reduce AC loss, it is different from the cable that mainly operates in DC condition. However, the lowest AC losses are not the goal of design. We also need to consider cost, reliability and maturity of manufacturing technology, etc. The Roebel cable is expensive to manufacture, so this conductor arrangement structure is not considered in the design of this cable.

(3) TSTC

The superconducting cable in the form of a single layer stack is too thick, which is not conducive to the uniformity of the electromagnetic. The feasible multi-strand TSTC scheme is shown in Table 1.

Table 1. Multi-strand TSTC scheme.

Label	Number of Strands	Number of Tapes per Strand	Number of Tapes	Size of Each Strand
TSTC-2	2	11	22	Φ 4.04
TSTC-3	3	7	21	Φ 4.11
TSTC-4	4	6	24	Φ 4.21

(4) Quasi-isotropic HTS strands

To ensure the uniformity of the quasi-isotropic HTS strands, the width and thickness of each strand stack should be nearly uniform. Since the width of the tape used is 4 mm, the thickness is 0.37 mm. Considering 0.1 mm polyimide insulation, the number of tapes included in each strand stack is approximately six. Therefore, the cable requires a total of four strand stacks to form a quasi-isotropic HTS strand.

(5) CICC

The CICC conductor adopts the same stacking form as the three-strand TSTC and the minimum inner radius of the conductor increases with the number of strands. Since there is a flow channel in the center of the CICC, if the number of strands is too small, the outer diameter of the cable skeleton will be too large. So, a relatively large number of strands are required, at least five strands and an inner radius of 10 mm.

4. Optimum Design of Cable Conductor Layout

4.1. Evaluation Index of Cable Performance

Considering the characteristics of different conductor layout methods, the conductor layout scheme for superconducting cables should be selected first. Based on the above design and simulation models of different conductor layout schemes, the following evaluation indicators of cable performance are formulated:

(1) Average external magnetic field $B_{\mathrm{avg\_out}}$

The performance of the cable mainly depends on its external magnetic field. The average magnetic induction intensity on the outer diameter of the cable is defined as the average external magnetic field $B_{\mathrm{avg\_out}}$ to describe the external characteristics of the cable.

(2) External magnetic field uniformity $B_{\mathrm{del\_out}}$

In order to facilitate the control of the effect in different parts, the radial and circumferential magnetic fields of the cable are required to be relatively uniform. The difference between the maximum magnetic induction intensity and the minimum magnetic induction intensity on the outer diameter of the cable is defined as the uniformity of the external magnetic field $B_{\mathrm{del\_out}}$, which is used to describe the uniformity of the external magnetic field of the cable. The smaller the $B_{\mathrm{del\_out}}$, the better the uniformity of the external magnetic field.

(3) Maximum magnetic field B_{max}

The magnetic field distributions generated by different conductor arrangements are different. On the basis of satisfying the external characteristics of the cable, the internal magnetic field of the cable is required to be as small as possible to reduce the impact on the cable body. Define the maximum magnetic induction intensity inside the cable as the maximum magnetic field B_{max}.

(4) Engineering critical current I_c

Under the influence of the magnetic field, the critical current of the tape degrades. Since the quench of superconducting tape has the characteristics of "point with line and line with surface", the critical current at the maximum magnetic field after the actual winding of the cable is taken as the engineering critical current I_c to describe the current-carrying capacity of the cable.

(5) Spatial-quantity ratio S/N

In order to meet the actual needs of light weight and miniaturization of cables, it is hoped that the volume of the cable should be as small as possible and the current-carrying capacity of the cable should be as large as possible. The ratio of the circular cross-sectional area S occupied by the cable conductor to the number of tapes N is defined as the spatial-quantity ratio and the space-quantity ratio needs to be as small as possible.

4.2. Performance Analysis of Different Conductor Layouts

Commonly used finite element simulation models for HTS cables include models based on H equation [20–22] and *T*-*A* equation [23–25]. Based on two different finite element solution methods and cable designs with different conductor layouts at 60 K, the corresponding finite element simulation models were built.

The performance analysis of superconducting cables with different conductor layouts is mainly aimed at the rated 4 kA working condition. Comparing the above two finite element solution methods, the H equation needs to consider the time operator t, which can only calculate the transient state, but cannot directly calculate the steady state. When evaluating the cable performance, it will waste a lot of computing resources and time. For the *T*-*A* equation, in addition to the transient calculation, it can also be directly applied to the steady state. So, it was chosen.

The 2G HTS tape has a high aspect ratio and the thickness of its superconducting layer is about 1 μm. It is a reasonable assumption to ignore the current flow in the tape thickness direction and consider only the current distribution in the tape width direction and the flow along the length direction. Therefore, by dimensionally reducing the tape in the thickness direction, the tape can be regarded as a two-dimensional surface. Furthermore, this is also the case when ignoring the influence of the axial magnetic field generated by the spiral structure on the tape performance. In the radial two-dimensional model of the cable, the tape is also reduced dimensionally in the thickness direction, making the geometric structure of the superconducting tape a one-dimensional curve. The control equation based on the *T*-equation is derived from Faraday's law, which is only used to calculate the current distribution on the conductor surface. The control equation based on the *A*-equation is derived from Ampere's law, which is applicable to the calculation of all regions of the magnetic field distribution. Both models are built and solved in COMSOL Multiphysics [26]. The *T*-equation model is solved in the PDE module, while the *A*-equation model is solved in the magnetic field module.

A equation is

$$\nabla \times \nabla \times A = \mu J \tag{5}$$

T equation is

$$J = \nabla \times T \tag{6}$$

Based on the *T*-*A* models of different cable structures, the performance of the cables is compared, as shown in Table 2. The steady-state magnetic field distribution is shown in Figure 7.

According to Table 2, when the currents are the same, the external magnetic fields of the cables with different structures are almost the same. For the CORC and the multi-strand TSTC and CICC structures, the difference between the maximum magnetic field and the minimum magnetic field on the outer Dewar surface of the cable is less than 1 mT, with high magnetic field uniformity. For a large current of 4 kA, the closer the conductor is to the axis, the larger the magnetic field and the larger the degradation of the critical current. Among them, the conductor of the CORC structure is far away from the axis. So, in terms of the critical current degradation, the CORC structure has greater advantages compared with TSTC, CICC and quasi-isotropic structures. Compared with the three-layer structure, the external magnetic field uniformity of the double-layer structure is higher and the maximum internal magnetic field is smaller. Therefore, it is recommended to use the double-layer CORC structure for the superconducting cable, as shown in Figure 8. At the same time, double corrugated pipes can be used to provide refrigerant channels in the cable core to increase the cooling capacity of the cable conductors and improve the space utilization of the system.

Table 2. Performance comparison of different conductor layouts.

Structure	B_{avg_out} (mT)	B_{del_out} (mT)	B_{max} (mT)	I_c (A)	S/N
CORC (2 layers)	32.054	0.471	38.856	115.81	26.66
CORC (3 layers)	32.095	0.705	54.852	107.39	13.242
TSTC (3 strands)	32.097	2.354	117.08	89.64	5.5779
TSTC (4 strands)	32.102	1.834	120.81	89.33	4.377
TSTC (5 strands)	32.102	0.473	123.54	89.24	3.4448
TSTC (6 strands)	32.101	0.553	109.53	90.01	3.9569
TSTC (8 strands)	32.103	0.447	101.62	93.58	4.5329
CICC (5 strands)	32.126	7.406	76.621	100.33	16.834
CICC (6 strands)	32.124	1.914	83.345	96.62	10.812
CICC (8 strands)	32.111	0.368	83.079	98.25	9.4444
Quasi-isotropic (2 strands)	32.098	6.7	122.93	88.96	5.9401

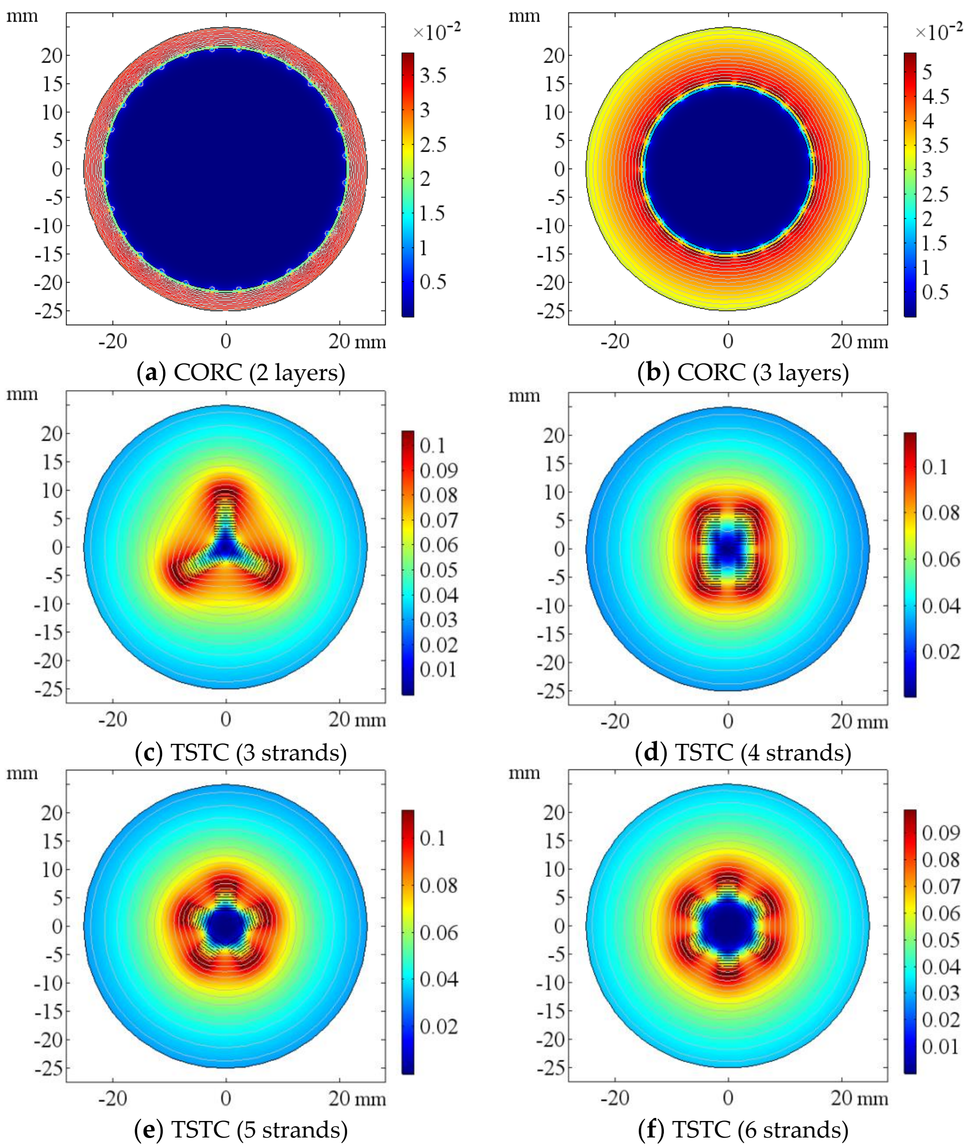

(**a**) CORC (2 layers) (**b**) CORC (3 layers)
(**c**) TSTC (3 strands) (**d**) TSTC (4 strands)
(**e**) TSTC (5 strands) (**f**) TSTC (6 strands)

Figure 7. *Cont.*

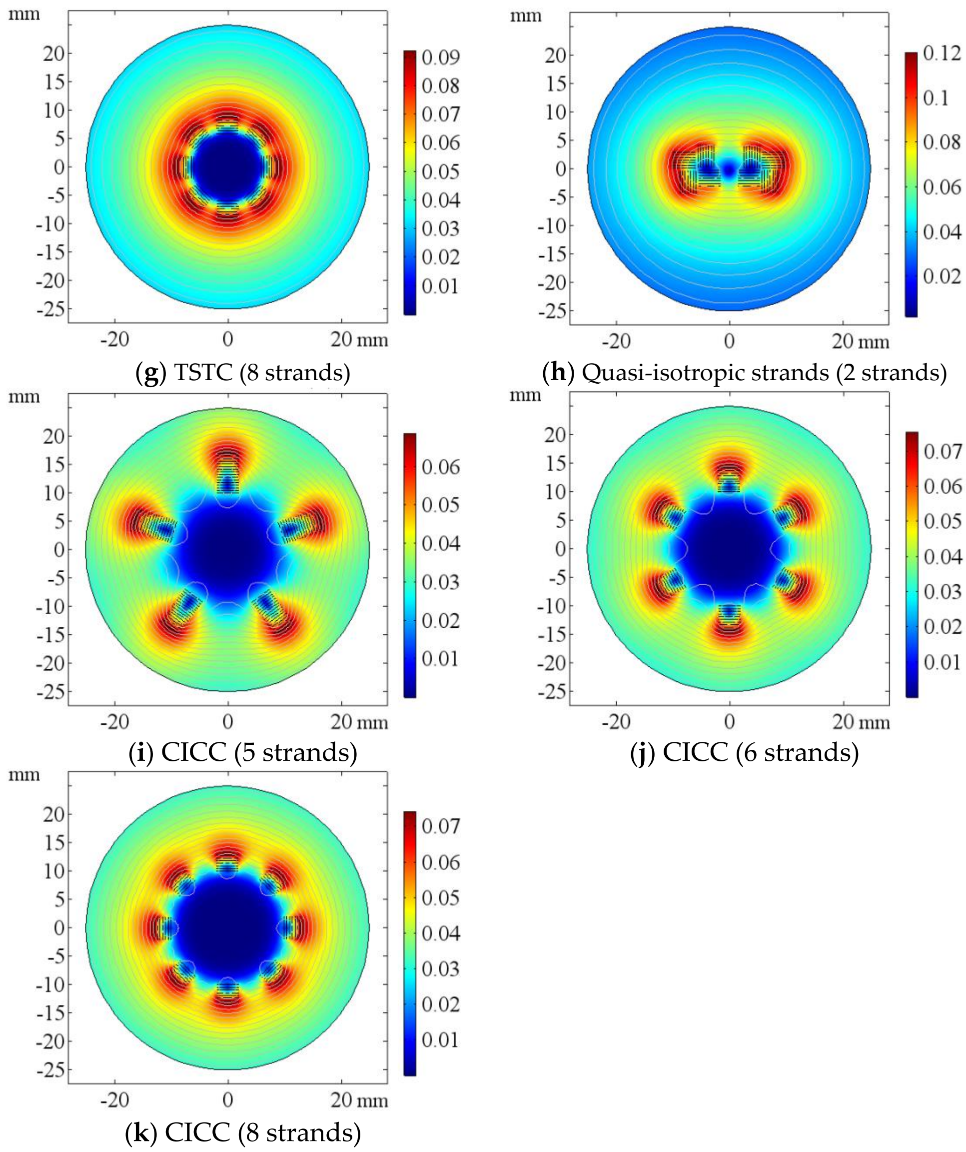

Figure 7. Magnetic field (T) on the surface of superconducting tape.

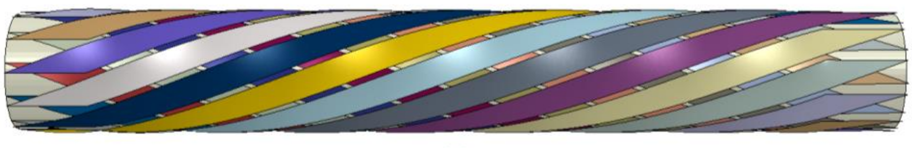

Figure 8. Topology diagram of double-layer CORC cable.

5. AC Loss Calculation

5.1. Simulation Method Validation

Taking a single tape as the research object, simulation and experimental comparison of AC loss were carried out. The AC loss measurement platform for superconducting tapes was built on the basis of the integration method. It can measure the current and the voltage of superconducting tapes under cyclic currents and can be used to measure their AC losses [27]. The SCS4050 tape produced by Superpower was used as the sample with a voltage lead measurement length of 22.5 cm. A sinusoidal alternating current was applied to the tape. The current range was 6 A–48 A, the step size was 7 A, the time range was 0 s–0.04 s and the step size was 0.001 s. The AC losses of superconducting tapes under different currents are shown in Figure 9. The results show that when a sinusoidal current is applied, the AC loss waveform presents a sinusoidal absolute value and the AC loss increases with the increase in the current amplitude. When the current amplitude is not large, the difference in AC loss under different currents is not large and as the current amplitude increases, the difference also increases. Figure 10 shows the average AC loss between simulation and experiment and the error between them. The error calculation formula is the quotient of the experimental value and the simulation value, and the larger the value, the greater the difference between the two. The results show that the error between the experiment and the simulation is generally about 4%, which shows that the AC loss can be evaluated accurately with this simulation method.

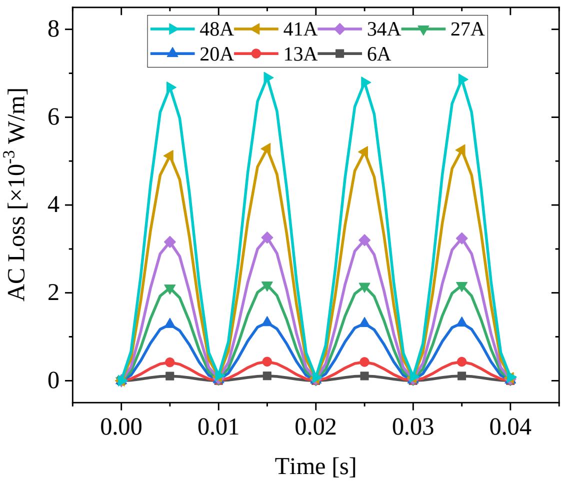

Figure 9. The AC loss of superconducting tapes under different currents.

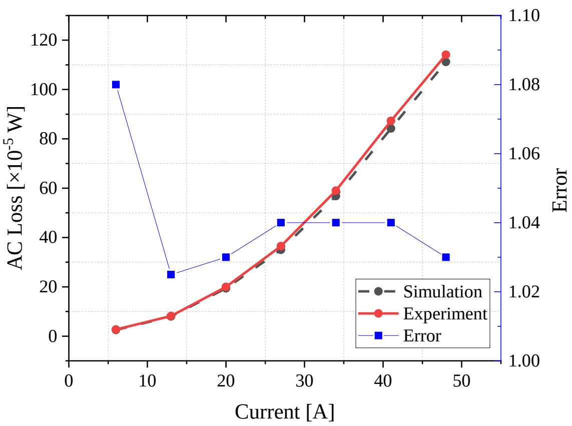

Figure 10. Comparison of AC Losses calculated by simulation and measured by experiment.

5.2. AC Loss Calculation for 60 K CORC Cable

The maximum working current of the cable is 4 kA, the decay rate is 10%, the pulse width is 2 s and the power-on interval is 2 s (the cycle is 8 s). When the current decays 30 times, the total current of the cable is 169.56 A, which is less than the critical current of a single tape. Therefore, the total flow time of the system was set to 15 cycles, 120 s. The reference waveform is shown in Figure 11. The loss generated by a complete process is calculated approximately:

$$Q_{\text{total}} = \sum_{i=0}^{i=30} P_i\left(0.9^i I_R\right) \times \Delta t \tag{7}$$

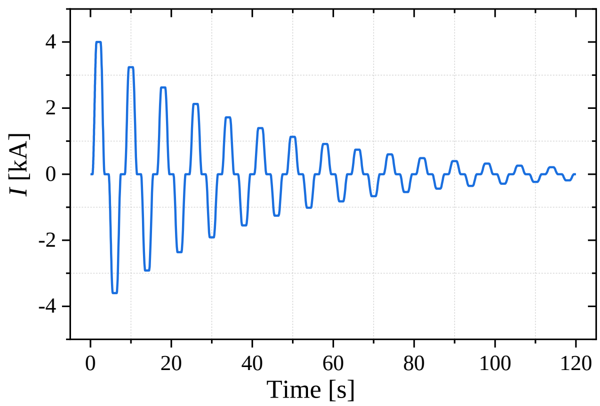

Figure 11. Current waveform of cable.

Among them, P_i is the power loss in one cycle and Δt is the steady-state current duration. The calculated total loss is about 9.81 J/m. The calculated loss of the cable under rated conditions is small and the heat dissipation capacity of the low-temperature system is greater than that. So, the cable can be guaranteed to work safely in the rated temperature range.

6. Conclusions

In this paper, the topology scheme of the HTS cable was designed and compared. Finally, the cable was determined to adopt a double-layer CORC structure and the AC loss under rated operating conditions was calculated. The following conclusions were obtained:

1. The characteristics of superconducting tapes were summarized: the lower the temperature and the smaller the magnetic field, the stronger the current-carrying capacity of the tape; under the same magnetic field, the critical current attenuation of the superconducting tape caused by the vertical magnetic field is significantly greater than that of the parallel magnetic field.
2. The parameters of HTS cables were determined first. The working temperature of the cable was selected to be 60 K, gaseous helium was used as the refrigerant and the number of tapes was at least 22. Superconducting cable conductors are laid out in multiple layers. The cable uses polyimide as the insulating material and is wrapped in a single layer with a thickness of 0.1 mm. The influence of rated voltage and cable length on the energized cross-section does not need to be considered. Then, the cable conductor layout methods of CORC, Roebel Cable, TSTC, CICC and quasi-isotropic structures were designed and finite element models under different layouts were built.
3. The average external magnetic field, the external magnetic field uniformity, the maximum magnetic field, the engineering critical current and the space quantity ratio were selected as the cable performance evaluation index indexes. The performance of different layouts was analyzed and CORC structure has advantages over other structures in terms of the maximum magnetic field and critical current attenuation inside the cable. Therefore, the CORC structure was selected.
4. The simulation model of superconducting cable was built based on *T-A* method and the AC loss of 60 K CORC cable was calculated. The cooling system can ensure the safe operation of the cable in the rated temperature range.

The cable design process was systematically given and the electromagnetic characteristics of cables with different topologies were comprehensively analyzed, providing guidance for the structural selection and design of cables. The difference in external magnetic field uniformity between the several cables is small and the differences in external magnetic field uniformity and maximum magnetic field strength are large. Superconducting conductor structure can be selected according to the specific application scenario of the cable.

Author Contributions: Conceptualization, S.P.; Methodology, S.P., C.C., J.Z.; Project administration, C.C.; Funding acquisition, C.C., J.Z., D.Z.; Investigation, S.P., J.C., D.Z.; Supervision, C.C., J.Z.; Validation, D.Z.; Visualization, S.P., J.C.; Writing-original draffy, S.P.; Writing-review& edit, D.Z. All authors have read and agreed to the published version of the manuscript.

Funding: This work is supported by the National Natural Science Foundation (Grant No. 52172271) and the Strategic Priority Research Program of the Chinese Academy of Sciences (Grant No. XDB2500-0000). China International Nuclear Fusion Energy Program (2022YFE03150200).

Data Availability Statement: The data presented in this study are available on request from the corresponding author. The data are not publicly available due to the confidentiality requirements of the project.

Conflicts of Interest: The authors declare no conflict of interest.

References

1. Kottonau, D.; de Sousa, W.T.B.; Bock, J.; Noe, M. Design Comparisons of Concentric Three-Phase HTS Cables. *IEEE Trans. Appl. Supercond.* **2019**, *29*, 5401508. [CrossRef]
2. Fetisov, S.S.; Zubko, V.V.; Zanegin, S.Y.; Nosov, A.A.; Ryabov, S.M.; Vysotsky, V.S. Study of the First Russian Triaxial HTS Cable Prototypes. *IEEE Trans. Appl. Supercond.* **2017**, *27*, 5400305. [CrossRef]
3. Angeli, G.; Bocchi, M.; Ascade, M.; Rossi, V.; Valzasina, A.; Martini, L. Development of Superconducting Devices for Power Grids in Italy: Update About the SFCL Project and Launching of the Research Activity on HTS Cables. *IEEE Trans. Appl. Supercond.* **2017**, *27*, 5600406. [CrossRef]
4. Lee, S.-J.; Sung, H.-J.; Park, M.; Won, D.; Yoo, J.; Yang, H.S. Analysis of the Temperature Characteristics of Three-Phase Coaxial Superconducting Power Cable according to a Liquid Nitrogen Circulation Method for Real-Grid Application in Korea. *Energies* **2019**, *12*, 1740. [CrossRef]
5. Nguyen, T.-T.; Lee, W.-G.; Lee, S.-J.; Park, M.; Kim, H.-M.; Won, D.; Yoo, J.; Yang, H.S. A Simplified Model of Coaxial, Multilayer High-Temperature Superconducting Power Cables with Cu Formers for Transient Studies. *Energies* **2019**, *12*, 1514. [CrossRef]
6. Nguyen, T.-T.; Lee, W.-G.; Kim, H.-M.; Yang, H.S. Fault Analysis and Design of a Protection System for a Mesh Power System with a Co-Axial HTS Power Cable. *Energies* **2020**, *13*, 220. [CrossRef]
7. Lee, S.-J.; Kang, S.Y.; Park, M.; Won, D.; Yoo, J.; Yang, H.S. Performance Analysis of Real-Scale 23 kV/60 MVA Class Tri-Axial HTS Power Cable for Real-Grid Application in Korea. *Energies* **2020**, *13*, 2053. [CrossRef]
8. Choi, Y.; Kim, D.; Lee, C.; Won, D.; Yoo, J.; Yang, H.; Kim, S. Thermo-Hydraulic Analysis of a Tri-Axial High-Temperature Superconducting Power Cable with Respect to Installation Site Geography. *Energies* **2020**, *13*, 3898. [CrossRef]
9. Huang, Z.; Wang, Y.; Lu, X.; Zhang, X.; Li, G.; Wang, L. A Multilayer Three-Phase Coaxial HTS Cable With Large Capacity and Low Loss. *IEEE Trans. Appl. Supercond.* **2022**, *32*, 4803007. [CrossRef]
10. Inoue, R.; Ueda, H.; Kim, S. Basic Study on Power Transmission Characteristics for High-Temperature Superconducting Cable Termination Applying a Wireless Power Transmission System. *IEEE Trans. Appl. Supercond.* **2022**, *32*, 5400804. [CrossRef]
11. Sadeghi, A.; Seyyedbarzegar, S.; Yazdani-Asrami, M. Investigation on the Electrothermal Performance of a High Temperature Superconducting Cable in an Offshore Wind Farm Integrated Power System: Fault and Islanding Conditions. *IEEE Trans. Appl. Supercond.* **2022**, *32*, 5401011. [CrossRef]
12. Oh, D.K. An Alternative in H-Formulation to the Critical Current Model of HTS Conductors. *IEEE Trans. Appl. Supercond.* **2022**, *32*, 4901808. [CrossRef]
13. Jacob, T.; Buchholz, A.; Noe, M.; Weil, M. Comparative Life Cycle Assessment of Different Cooling Systems for High-Temperature Superconducting Power Cables. *IEEE Trans. Appl. Supercond.* **2022**, *32*, 4802805. [CrossRef]
14. Tang, T.; Zong, X.H.; Yu, Z.G.; Lu, X.H.; Han, Y.W. Design and operation of cryogenic system for 35kV/2000A HTS power cables. In Proceedings of the 2015 IEEE International Conference on Applied Superconductivity and Electromagnetic Devices (ASEMD), Shanghai, China, 20–23 November 2015; pp. 573–575. [CrossRef]
15. HTS Wire Critical Current Database. Available online: https://htsdb.wimbush.eu/ (accessed on 1 November 2021).
16. Rossi, L.; Hu, X.; Kametani, F.; Abraimov, D.; Polyanskii, A.; Jaroszynski, J.; Larbalestier, D.C. Sample and length-dependent variability of 77 and 4.2 K properties in nominally identical RE123 coated conductors. *Supercond. Sci. Technol.* **2016**, *29*, 054006. [CrossRef]
17. Kubiczek, K.; Grilli, F.; Kario, A.; Godfrin, A.; Zermeno, V.; Stepien, M.; Kampik, M. Length Uniformity of the Angular Dependences of I_c and n of Commercial REBCO Tapes with Artificial Pinning at 77 K. *IEEE Trans. Appl. Supercond.* **2019**, *29*, 8000309. [CrossRef]
18. Zhang, H.; Zhu, J.; Xu, W.; Zhu, C.; Zhang, H.; Deng, X. Design of three-phase coaxial cold insulated superconducting cable. *Cryog. Supercond.* **2019**, *47*, 10.
19. Van der Laan, D.C. YBa2Cu3O7−delta coated conductor cabling for low ac-loss and High-field magnet applications. *Supercond. Sci. Technol.* **2009**, *22*, 065013. [CrossRef]

20. Zhang, M.; Coombs, T.A. 3D modeling of high-Tc superconductors by finite element software. *Supercond. Sci. Technol.* **2011**, *25*, 015009. [CrossRef]
21. Sheng, J.; Vojenčiak, M.; Terzioglu, R.; Frolek, L.; Gömöry, F. Numerical study on magnetization characteristics of superconducting conductor on round core cables. *IEEE Trans. Appl. Supercond.* **2016**, *27*, 4800305. [CrossRef]
22. Terzioğlu, R.; Vojenčiak, M.; Sheng, J.; Gömöry, F.; Çavuş, T.F.; Belenli, İ. AC loss characteristics of CORC cable with a Cu former. *Supercond. Sci. Technol.* **2017**, *30*, 085012. [CrossRef]
23. Zhang, H.; Zhang, M.; Yuan, W. An efficient 3D finite element method model based on the T–A formulation for superconducting coated conductors. *Supercond. Sci. Technol.* **2016**, *30*, 024005. [CrossRef]
24. Wang, Y.; Zhang, M.; Grilli, F.; Zhu, Z.; Yuan, W. Study of the magnetization loss of CORC cables using a 3D TA formulation. *Supercond. Sci. Technol.* **2019**, *32*, 025003. [CrossRef]
25. Zermeño, V.M.R.; Habelok, K.; Stępień, M.; Grilli, F. A parameter-free method to extract the superconductor's $J_c(B,\theta)$ field-dependence from in-field current–voltage characteristics of high temperature superconductor tapes. *Supercond. Sci. Technol.* **2017**, *30*, 034001. [CrossRef]
26. COMSOL Inc. Available online: https://cn.comsol.com/ (accessed on 1 February 2022).
27. Zhu, K.; Guo, S.; Ren, L.; Xu, Y.; Wang, F.; Yan, S.; Liang, S.; Tang, Y.; Shi, J.; Li, J. AC loss measurement of HTS coil under periodic current. *Phys. C Supercond. Its Appl.* **2020**, *569*, 1353562. [CrossRef]